Human Molecular Genetics, 2007, Vol. 16, No. 22 ***2693–2702***
doi:10.1093/hmg/ddm223
Advance Access published on August 27, 2007

Functional correction of CNS lesions in an MPS-IIIA mouse model by intracerebral AAV-mediated delivery of *sulfamidase* and *SUMF1* genes

Alessandro Fraldi[1,*†], Kim Hemsley[2,†], Allison Crawley[2], Alessia Lombardi[1], Adeline Lau[2], Leanne Sutherland[2], Alberto Auricchio[1,3], Andrea Ballabio[1,3] and John J. Hopwood[2]

[1]Telethon Institute of Genetics and Medicine (TIGEM), 80131 Naples, Italy, [2]Department of Genetic Medicine, Children, Youth and Women's Health Service, Lysosomal Diseases Research Unit, Adelaide 5006, Australia, [3]Medical Genetics, Department of Pediatrics, Federico II University, Naples, Italy

Received June 25, 2007; Revised and Accepted August 12, 2007

Mucopolysaccharidosis type IIIA (MPS-IIIA or Sanfilippo syndrome) is a lysosomal storage disorder caused by the congenital deficiency of sulfamidase (SGSH) enzyme and consequent accumulation of partially degraded heparan sulfate (HS) in lysosomes. The central nervous system (CNS) is the predominant site of tissue damage in MPS-IIIA. Here we describe a gene therapy approach for MPS-IIIA in a mouse model using recombinant adeno-associated virus serotype 5 (AAV2/5) as a vehicle to deliver therapeutic genes to the CNS. SUMF1 (SUlfatase Modifying Factor 1) exhibits an enhancing effect on sulfatase activity when co-expressed with sulfatases. Consistent with these findings, we demonstrated that co-delivery of SUMF1 and SGSH (via an AAV2/5-CMV-SGSH-IRES-SUMF1 vector) resulted in a synergistic increase in SGSH activity, both in primary neural cells and in murine brain. A study aimed at testing the therapeutic efficacy of simultaneous brain administration of SUMF1 and SGSH was then performed by injecting the lateral ventricles of newborn MPS-IIIA/normal mice with either AAV2/5-CMV-SGSH-IRES-SUMF1 or AAV2/5-CMV-GFP vectors. Widespread GFP expression was observed within the GFP-injected brain, and a stable and significant increase of SGSH activity was detected in several brain regions following SGSH-IRES-SUMF1 administration. Treatment with AAV2/5-CMV-SGSH-IRES-SUMF1 vectors resulted in a visible reduction in lysosomal storage and inflammatory markers in transduced brain regions. Finally, the MPS-IIIA mice treated with therapeutic genes displayed an improvement in both motor and cognitive functions. Our results suggest that early treatment of CNS lesions by AAV-mediated intraventricular injection of both *SGSH* and *SUMF1* genes may represent a feasible therapy for MPS-IIIA.

INTRODUCTION

Deficiency of lysosomal hydrolases causes the storage of intermediate catabolites in lysosomes. This results in chronic and progressive conditions known as lysosomal storage disorders (LSDs). LSDs comprise more than 45 monogenic disorders characterized by a wide spectrum of clinical problems, leading to organ dysfunction and early mortality (1). Mucopolysaccharidosis type IIIA (MPS-IIIA or Sanfilippo syndrome) belongs to a subgroup of LSDs, the mucopolysaccharidoses (MPSs), that are caused by the deficiency of lysosomal enzymes responsible for the catabolism of glycosaminoglycans (2). MPS-IIIA arises from the congenital loss of function of sulfamidase (SGSH), a sulfatase enzyme involved in the step-wise degradation of heparan sulfate (HS). There are three other subtypes of MPS-III (B, C and D), all of which are caused by deficiencies in different enzymes required for HS catabolism. MPS-IIIA is the most frequent subtype in some populations and is also the most common of the MPS disorders (3).

In many LSDs, and in MPS-IIIA in particular, the central nervous system (CNS) is the predominant site of pathology. In fact, although the somatic organs are affected in

*To whom correspondence should be addressed at: Telethon Institute of Genetics and Medicine (TIGEM), Via P. Castellino, 111, 80131 Naples, Italy. Tel: +39 0816132218; Fax: +39 0815609877; Email: fraldi@tigem.it
†The authors wish it to be known that, in their opinion, the first two authors should be regarded as joint First Authors.

MPS-IIIA, the dominant clinical features are neurological dysfunction and neurocognitive decline. As a result, patients experience a wide range of symptoms, including delayed development, mental retardation, rapid loss of social skills and learning ability, disturbed sleep, aggression and hyperactivity (2).

Currently, there are two canine models (4,5) and a murine model (6,7) with SGSH deficiency. The MPS-IIIA mouse model results from a spontaneous missense mutation (D31N) in the catalytic site of the SGSH enzyme that reduces its activity to ~3% of normal mouse (8). MPS-IIIA mice exhibit HS storage from birth (7,9); by 3 weeks of age, become hyperactive; and from ~10 weeks, start to display aggressive behavior (10). As the disease advances, a hunched posture together with hepato-splenomegaly is observed. The affected mice also become less active and death is common by ~12 months of age (6,10). Disease progression in MPS-IIIA mice is similar to that observed in MPS-IIIA patients, making the mice an excellent model for evaluating the pathogenic mechanisms of disease and for the development of therapeutic strategies (7,10).

No effective and safe clinical therapies for MPS-IIIA patients have been reported to date. Hematopoietic stem cell transplantation or bone marrow transplantation represent effective treatment options for several LSDs involving the CNS, but have been largely unsuccessful in MPS-III patients for reasons that are not well understood. In addition, enzyme replacement therapy (ERT) protocols are currently available for Gaucher, Fabry and Pompe diseases, MPS-I, MPS-II and MPS-VI. ERT at traditional doses is not expected to treat CNS disease.

Although high-dose intravenous ERT could potentially provide treatment for CNS disease (11), the extent of clinical improvement in CNS signs following high-dose ERT in MPS disorders is, as yet, untested. Another long-term and potentially once-off therapeutic strategy is gene therapy. Recombinant adeno-associated virus (rAAV) vectors offer a high level of safety combined with clinical efficacy and versatility in terms of potential applications (12). Moreover, rAAV vectors are capable of efficiently transducing non-dividing cells in the absence of pathogenic or inflammatory effects (13), and they have been shown to be effective as therapeutic agents for the treatment of neuropathological lesions in several MPS diseases (14–16).

In the present study, we tested the therapeutic efficacy of rAAV serotype 5 as a tool to deliver both *SUMF1* (SUlfatase Modifying Factor 1) and *SGSH* genes directly to the CNS of newborn MPS-IIIA mice. SUMF1 is the enzyme that catalyzes the post-translational modification of a cysteine residue located within the sulfatase active site into α-formylglycine, resulting in sulfatase activation (17,18). Indeed, in a rare autosomal recessive disorder, multiple sulfatase deficiency, the activity of all sulfatases is profoundly impaired owing to SUMF1 deficit (19). We and other groups have previously shown that simultaneous over-expression of SUMF1 and human sulfatase cDNA results in a strikingly synergistic increase in enzyme activity of each sulfatase examined, both *in vitro* and *in vivo*, indicating that SUMF1 is both an essential and a limiting factor for sulfatases (17,20,21). The results obtained here demonstrate that a reduction in pathological brain lesions and an improvement in behavioral phenotype is possible in MPS-IIIA mice following treatment with rAAV expressing both SUMF1 and SGSH.

RESULTS

Determination of SUMF1-enhancing effect on SGSH activity in murine primary cultured neural cells and in the murine brain

Primary neural cells derived from newborn normal (heterozygotes, phenotypically unaffected) and MPS-IIIA mice were infected with AAV2/5-CMV vectors expressing GFP, SGSH, or both SGSH and SUMF1 genes. The contemporaneous expression of SGSH and SUMF1 proteins was achieved by using an IRES cassette between SGSH and SUMF1 cDNAs (AAV2/5-CMV-SGSH-IRES-SUMF1). Five days after infection, GFP-infected normal neural cells displayed ~10-fold higher enzyme activity with respect to GFP-infected MPS-IIIA cells (Fig. 1A). A significant increase in SGSH activity ($P < 0.05$) was observed in both normal and MPS-IIIA neural cells after infection with AAV encoding SGSH alone (Fig. 1A). The co-expression of SUMF1 together with SGSH via AAV2/5-CMV-SGSH-IRES-SUMF1 transduction led to a significant additional increase in SGSH activity ($P < 0.05$) (Fig. 1A).

To substantiate the enhancing effect of SUMF1 *in vivo*, we tested the effect of simultaneous delivery of both SGSH and SUMF1 versus SGSH alone in the murine brain. To this end, newborn normal and MPS-IIIA mice received microinjections of 6×10^9 particles of AAV2/5-CMV-SGSH-IRES-SUMF1, AAV2/5-CMV-SGSH or AAV2/5-CMV-GFP bilaterally into the lateral ventricles. Six weeks post-injection, examination of tissue sections revealed that the most rostral brain slice from GFP-injected mice was the most intensely stained and thus the most efficiently transduced. SGSH activity was then measured in this hemi-coronal segment (see diagram in Fig. 1B). SGSH activity in normal GFP-injected mouse brain was ~16-fold higher compared with the amount detected in the GFP-injected MPS-IIIA mice (Fig. 1B). A 2-fold increase in enzyme activity was observed following SGSH administration to MPS-IIIA mouse brain, and the simultaneous delivery of SGSH and SUMF1 resulted in an additional 1.5-fold increase in enzyme activity ($P < 0.05$) (Fig. 1B). Notably, neither SGSH nor SGSH-IRES-SUMF1 produced a significant increase in SGSH activity in the normal mouse brain (Fig. 1B).

Effect of AAV2/5-mediated delivery of *SGSH* and *SUMF1* genes on the clinical and neuropathological course of disease in the MPS-IIIA mouse

The therapeutic efficacy of AAV-mediated simultaneous delivery of SUMF1 and SGSH to the CNS of newborn MPS-IIIA mice was then examined. Either AAV2/5-CMV-SGSH-IRES-SUMF1 or AAV2/5-CMV-GFP vectors (3×10^{10} viral particles) were administered bilaterally to the ventricles of both unaffected and affected newborn mice.

AAV2/5-mediated transgene expression in mouse brain At 6 weeks post-injection, brain sections from MPS-IIIA and

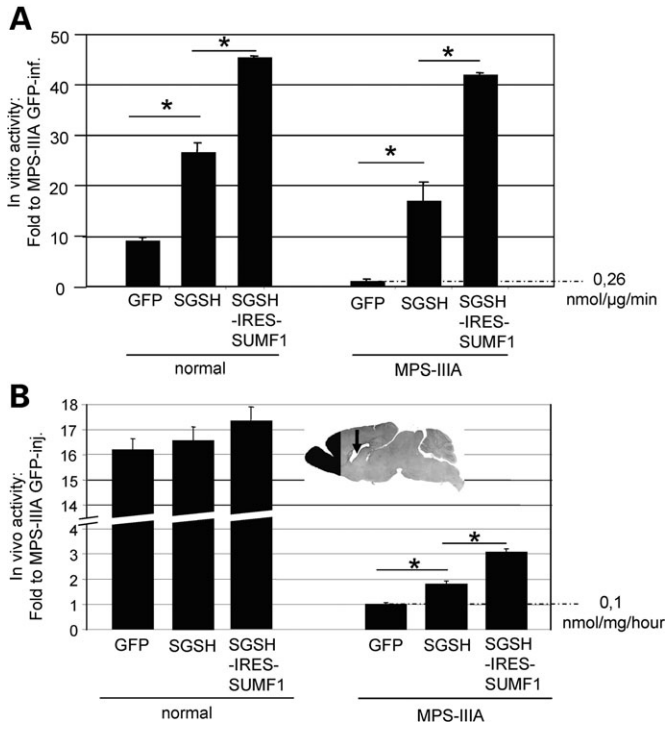

Figure 1. Effect of SUMF1 on SGSH activity in primary cultured brain cells and in the brain of normal and MPS-IIIA mice. AAV2/5-CMV-GFP, AAV2/5-CMV-SGSH or AAV2/5-CMV-SGSH-IRES-SUMF1 vectors were used to infect neural cells derived from normal and MPS-IIIA mice (**A**) or were intraventricularly injected into the brain of both normal and MPS-IIIA mice at birth (**B**). Arrow in the diagram indicates the injection site. An anterior coronal brain slice (2 mm thick) containing the olfactory bulb and rostral cerebral cortex (black region in the diagram) was removed 6 weeks post-injection and used to quantify SGSH activity. Enzyme activity is expressed as the fold-level of the activity detected in GFP-treated MPS-IIIA cells or brain. Each bar represents the average of three independent infections or of the activity measured in three to four different injected mice. Error bars: ± 1 SEM. ($^*P < 0.05$).

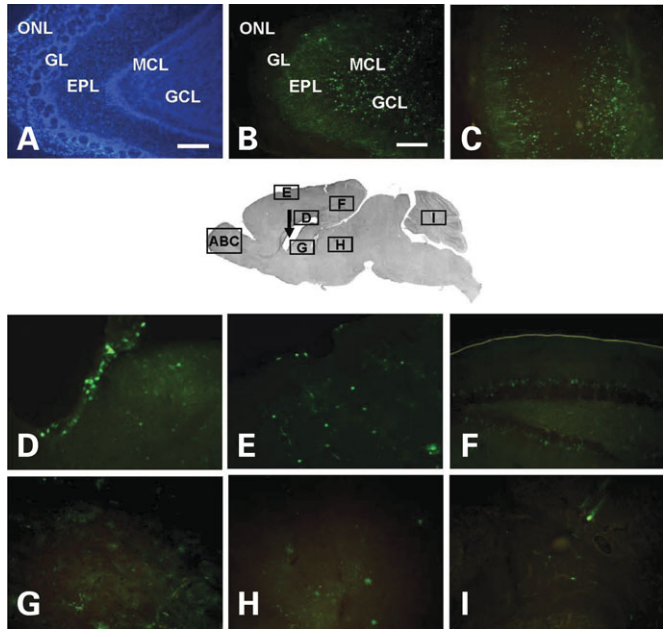

Figure 2. Distribution of GFP in the mouse brain after AAV2/5-mediated intraventricular injection. The GFP expression was detected in various brain regions in AAV2/5-CMV-GFP-injected mice at 6 weeks (**B** and **D**–**G**), 12 weeks (**H** and **I**) and 22 weeks (**C**) post-injection. DAPI (**A**) and GFP staining (B and C) demonstrated that the olfactory bulb was the most strongly transduced region, with GFP expression detectable in most of the olfactory bulb cell layers. ONL, olfactory nerve layer; GL, glomerular layer; EPL, external plexiform layer; MCL, mitral cell layer; GCL, granular cell layer. The choroid plexus (D), the cerebral cortex (above the ventricle) (E) and, at less extent, the dentate gyrus of the hippocampus (F) and the striatum (G) were also efficiently transduced (D–G). A low but significant GFP expression was evident in the thalamus (H) and in both the Purkinje cell neurons and cerebellar nuclei (I). Scale bar: 60 µm. The arrow indicates the injection site.

normal GFP-injected mice revealed that the olfactory bulb was the most efficiently transduced region (Fig. 2A and B). The choroid plexus in the lateral ventricle was also strongly transduced, whereas less-intense GFP expression was also detected in the cerebral cortex (above the ventricle), in the dentate gyrus of the hippocampus and in the striatum (Fig. 2D–G). At 12 weeks post-injection, a similar distribution of GFP-positive cells remained, with the addition of low but significant GFP expression that became evident in the thalamus (Fig. 2H) and in both the Purkinje cell neurons and cerebellar nuclei (Fig. 2I). At 5 months post-injection, GFP expression persisted vigorously in the olfactory bulb, and fluorescence was also observed in other brain regions such as the choroid plexus, cerebral cortex and striatum (Fig. 2C; data not shown).

SGSH activity was then determined in brain extracts, following dissection of the brain into five coronal slices (anterior to posterior: A, B, C, D, E; see brain sections in Fig. 3). Consistent with the results described earlier, in all five brain slices and at all ages examined, SGSH activity in normal mice (GFP-treated) was 13- to 16-fold greater than that measured in GFP-injected MPS-IIIA mice (Fig. 3); no significant difference was observed between GFP-treated and SGSH-IRES-SUMF1-treated normal mice (data not shown). A 2- to 3-fold increase in SGSH activity was observed in SGSH-IRES-SUMF1-treated (versus GFP-treated) MPS-IIIA mice in the anterior segments of brain from 6 weeks post-injection, which persisted until at least 22 weeks post-injection (Fig. 3). The distribution of enzyme activity in SGSH-IRES-SUMF1-treated MPS-IIIA mice correlated well with the GFP staining in GFP-injected mice: for example, slice A contains the olfactory bulb, and slices B and C contain the choroid plexus, parts of cerebral cortex, striatum and hippocampus, structures that contained GFP-positive cells; conversely, slices D and E had no detectable increase in SGSH activity and comprised brainstem regions and cerebellum, in which the GFP signal was absent or only present at very low levels.

Correction of neuropathological storage in SGSH-IRES-SUMF1-treated MPS-IIIA mice MPS-IIIA mice injected with AAV2/5-CMV-SGSH-IRES-SUMF1 along with normal and MPS-IIIA GFP-treated mice were assessed for the presence of pathological storage in the brain. Electron microscopy (EM) analysis of GFP-treated MPS-IIIA mouse brain showed, at all ages examined, a picture of pathological accumulation similar to that previously reported (6,7,22): glial cells exhibited large electron-dense vacuoles, in some cases containing granular material (Fig. 4B); olfactory bulb mitral cells and pyramidal

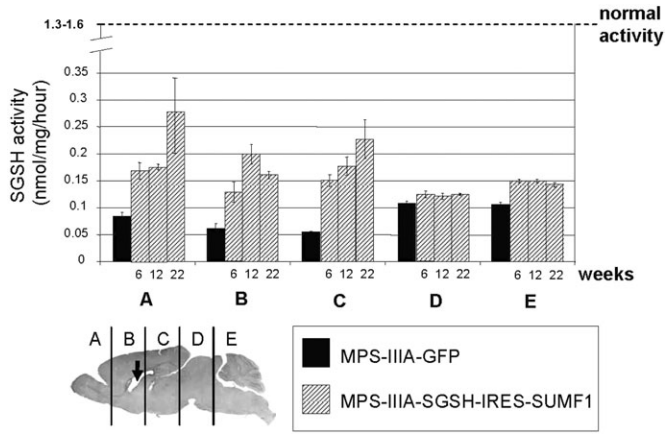

Figure 3. SGSH activity in the mouse brain after AAV2/5-mediated intraventricular injection. SGSH activity was measured 6, 12 and 22 weeks post-injection in the extracts of five hemi-coronal brain segments (see brain diagram) derived from the four treatment groups. Activity was expressed as nanomoles of enzyme normalized against protein content (mg) and incubation time (h). Each bar represents the average of two (in the 6- and 12-week measurements) or three (in the 22-week measurements) injected mice. Error bars: ± 1 SEM. The arrow indicates the injection site.

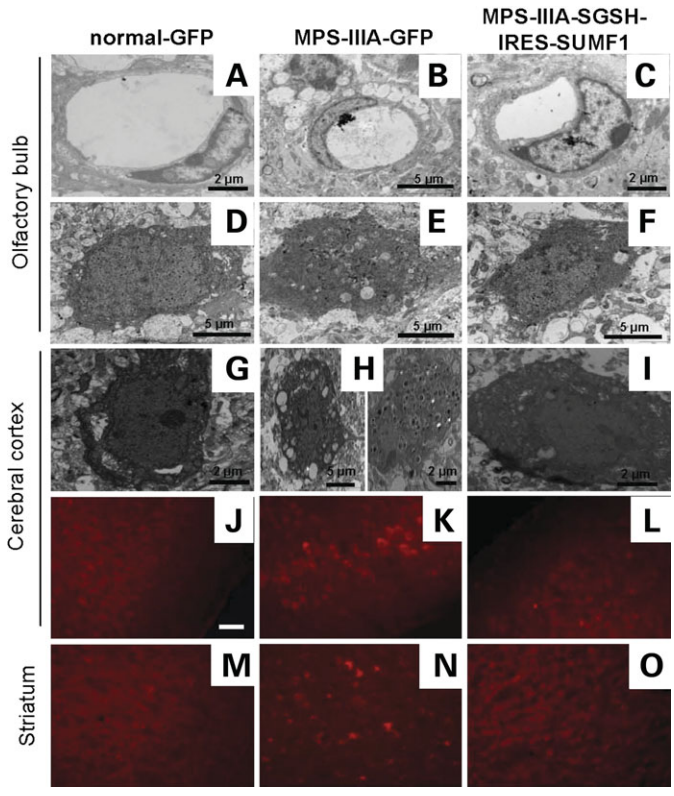

Figure 4. Evaluation of neuropathological storage in injected mice. EM images of glial perivascular cells (**A**–**C**) and mitral cells (**D**–**F**) of the olfactory bulb of normal GFP-treated (A and D), MPS-IIIA GFP-treated (B and E) or MPS-IIIA SGSH-IRES-SUMF1-treated mice (C and F) taken 6 weeks post-injection. EM images of cortical pyramidal neurons of normal GFP-treated (**G**), MPS-IIIA GFP-treated (**H**) or MPS-IIIA SGSH-IRES-SUMF1-treated mice (**I**) taken 12 weeks post-injection. Extensive vacuolation was present throughout the brain of GFP-treated MPS-IIIA mice, and membranous inclusions were also evident (B, E and H). Neurons and glia of MPS-IIIA mice treated with SGSH-IRES-SUMF1 showed a clear reduction of vacuolation and inclusions at all ages analyzed (C, F and I). GM2 immunofluorescence staining is shown in the cerebral cortex (**J**–**L**) and striatum (**M**–**O**) of GFP-treated normal mice (J and M), GFP-treated MPS-IIIA mice (K and N) or SGSH-IRES-SUMF1-treated MPS-IIIA mice (L and O). Images were taken 12 weeks (J, K and L) and 22 weeks (M, N and O) after injection. A reduction of GM2 storage was observed in the brains of MPS-IIIA mice upon treatment with SGSH-IRES-SUMF1 (L and O). Scale bar for (J–O): 30 μm.

neurons in the cerebral cortex displayed a mixed population of electron-lucent vacuoles and 'zebra body' inclusions (Fig. 4E and H). No storage pathology was evident in GFP-treated normal mouse brain (Fig. 4A, D and G). Treatment with AAV vectors expressing SGSH-IRES-SUMF1 resulted in a significant reduction in vacuolization in both glial and neuron cells of the examined brain regions at all ages analyzed (Fig. 4C, F and I). A semi-quantitative analysis of pathological storage was performed in the cerebral cortex in 12-week-old mice. We examined one mouse for each treatment group and counted 50 neurons and 50 glial cells per mouse. We found that the number of neurons with storage material decreased by $\sim$90% with respect to GFP-injected MPS-IIIA mice, and, where present, the vacuoles were smaller in size and number. The reduction in storage was less evident in glia, with about a 20% reduction in the number of glia with vacuoles.

Although the accumulation of HS represents the primary outcome in MPS-IIIA, GM2 and GM3 gangliosides secondarily accumulate in this and other MPS disorders (23). Consistent with these findings, anti-GM2 immunofluorescence was observed in brain sections taken from the cerebral cortex (Fig. 4K) and the striatum (Fig. 4N) of both 12- and 22-week-old GFP-injected MPS-IIIA mice. The fluorescence signal was undetectable in brain sections taken from the same regions in normal mouse brain (Fig. 4J and M) and appeared greatly reduced in the corresponding regions of SGSH-IRES-SUMF1-treated MPS-IIIA mouse brain (Fig. 4L and O).

Reduction of inflammation in SGSH-IRES-SUMF1-treated MPS-IIIA mice MOMA-2 specifically marks activated macrophages during the inflammatory process (24). Brain sections from both 12- and 22-week-old GFP-treated unaffected mice revealed a complete lack of MOMA-2 immuno-reactivity in all areas examined (Fig. 5A, E and I; data not shown). Conversely, in the corresponding areas of 12-week-old GFP-treated MPS-IIIA mice, a large number of MOMA-2 immuno-positive cells were detected, thus revealing a massive activation of microglia throughout the CNS of affected mice (Fig. 5B, F and J; data not shown). An increase in both number and extent of MOMA-2 staining was observed with age (Fig. 5B, F and J versus C, G and K). Notably, the MOMA-2 staining appeared to depict many macrophages in close association with neurons, consistent with EM observations (Fig. 5M and N). Treatment with AAV vectors expressing both SGSH and SUMF1 reduced microglial activation in both the cerebral cortex and the striatum in affected mice (Fig. 5D and H). However, some areas such as the cerebellum and brainstem showed no difference in MOMA-2 staining following SGSH-IRES-SUMF1 treatment (Fig. 5L; data not shown). These regions partially overlapped with the brain areas that were not significantly transduced upon AAV-mediated delivery.

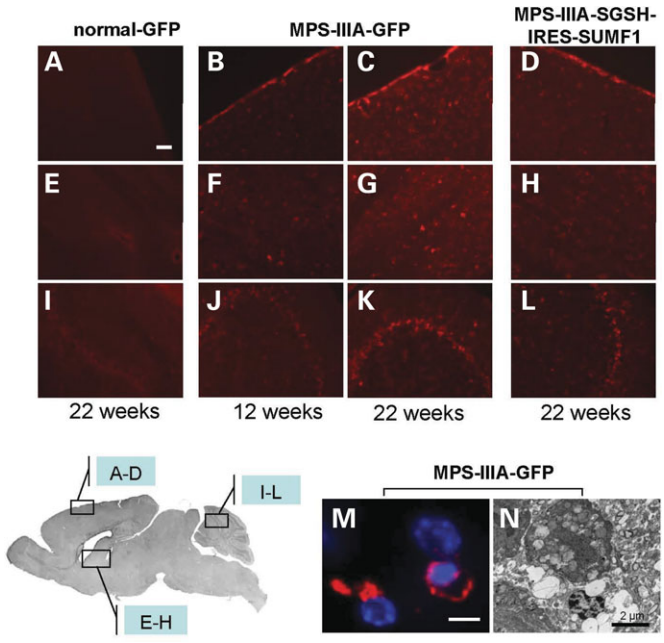

Figure 5. Reduction of microglial activation in the brain of SGSH-IRES-SUMF1-treated MPS-IIIA mice. MOMA-2 immunofluorescence revealed a massive activation of microglia in the cerebral cortex (**B** and **C**), striatum (**F** and **G**) and cerebellum (**J** and **K**) of GFP-treated MPS-IIIA mice. The microglial activation increased with age (B, F and J versus C, G and K). Higher magnification imaging of sections double-stained with MOMA-2 and DAPI revealed macrophages (MOMA-2 positive; red) juxtaposed to neurons (nuclei stained with DAPI only; blue) (**M**). Perineuronal macrophages were also observed at the EM level (**N**). No signs of macrophage activation were observed in the brain of normal GFP-treated mice (**A**, **E** and **I**). Treatment with SGSH-IRES-SUMF1 resulted in a reduction of microglial activation (MOMA-2-positive cells) in both the cerebral cortex and striatum (**D** and **H**) but not in the cerebellum (**L**) of MPS-IIIA mice. Images were taken at locations shown in the diagram. Scale bar: 30 μm in (A–L), and 12 μm in (M).

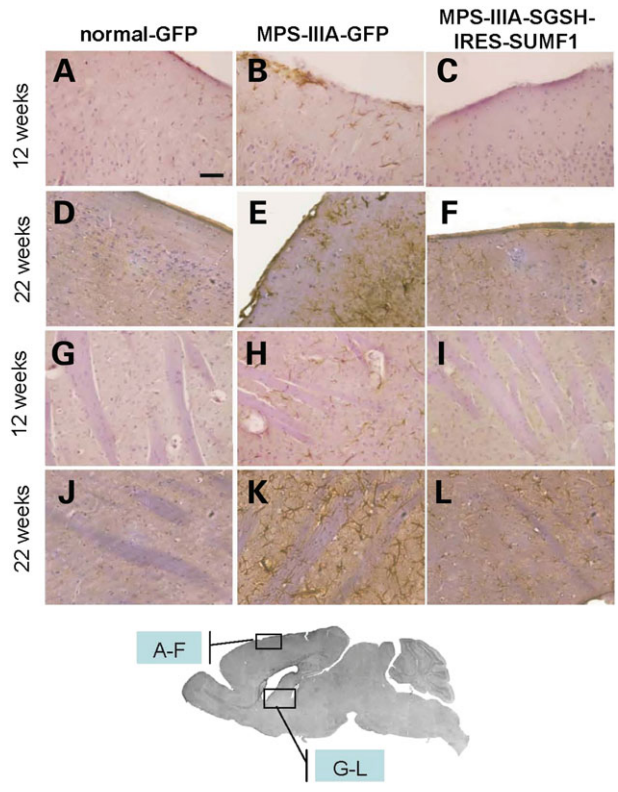

Figure 6. Amelioration of astrogliosis in the brain of SGSH-IRES-SUMF1-treated MPS-IIIA mice. Immunohistochemical staining of GFAP in GFP-treated MPS-IIIA mice exhibited a diffuse astrogliosis that was particularly evident in the cerebral cortex (**B** and **E**) and striatum (**H** and **K**), compared with the same regions in normal GFP-treated mice (**A**, **D**, **G** and **J**). The number of GFAP-positive glia increased with age (B and H versus E and K). A reduction in astrogliosis was observed in the cerebral cortex and striatum of MPS-IIIA mice treated with SGSH-IRES-SUMF1 (**C**, **F**, **I** and **L**). Images were taken at locations shown in the diagram. Scale bar: 30 μm.

Immunostaining with an anti-GFAP antibody that specifically stains reactive astrocytes showed a diffuse immunoreactivity in several brain areas, and the difference between normal and MPS-IIIA mice was a matter of degree, as previously reported (25). The cerebral cortex and striatal regions most clearly indicated a difference between GFP-treated affected mice and normal mice. In fact, at both 12 and 22 weeks of age, we observed a very strong GFAP immunoreactivity in both the cerebral cortex and striatal regions of affected GFP-treated mice (Fig. 6B, E, H and K), whereas the normal mice exhibited a low immunoreactivity (Fig. 6A, D, G and J). The astrogliosis increased with age (Fig. 6E and K versus B and H) and was reduced in MPS-IIIA mouse brain upon SGSH-IRES-SUMF1 treatment (Fig. 6C, F, I and L).

Behavioral assessment To determine the effect of AAV transduction on motor and cognitive deficits in affected mice, we undertook three different behavioral tests on male mice at different ages after treatment at birth. Hind-limb gait was determined with a footprint test at 18 weeks, which revealed a significant reduction ($P < 0.05$) in both gait length and width in MPS-IIIA GFP-treated mice compared with normal (GFP- and SGSH-IRES-SUMF1-treated) mice. The treatment of MPS-IIIA mice with the AAV-SGSH-IRES-SUMF1 vector resulted in the recovery ($P < 0.05$) of normal gait (Fig. 7A). Open-field locomotor activity was measured 10, 15, 18 and 21 weeks after AAV injection. The activity in all mice generally decreased from 10 to 18 weeks, and during this time, no significant differences were observed between normal and MPS-IIIA mice regardless of the treatment (Fig. 7B). At 21 weeks of age, the MPS-IIIA GFP-treated mice became significantly more active ($P < 0.05$) compared with normal (GFP- and SGSH-IRES-SUMF1-treated) mice, whereas the MPS-IIIA mice treated with SGSH-IRES-SUMF1 showed exploratory activity similar to that observed in normal mice (Fig. 7B).

Finally, we evaluated the effect of treatment on memory and spatial learning capability using the Morris water maze (MWM) test. During the first 2 days of the test (visual phase), no significant differences in either visual ability or swim speed were observed among groups (Fig. 7C). Consistent with previous findings (7,22), the acquisition phase revealed an impaired spatial learning function in affected mice. In fact, although on the first day of the acquisition phase (day 3 of testing) all mice exhibited similar latencies to reach the platform, on subsequent days, MPS-IIIA mice

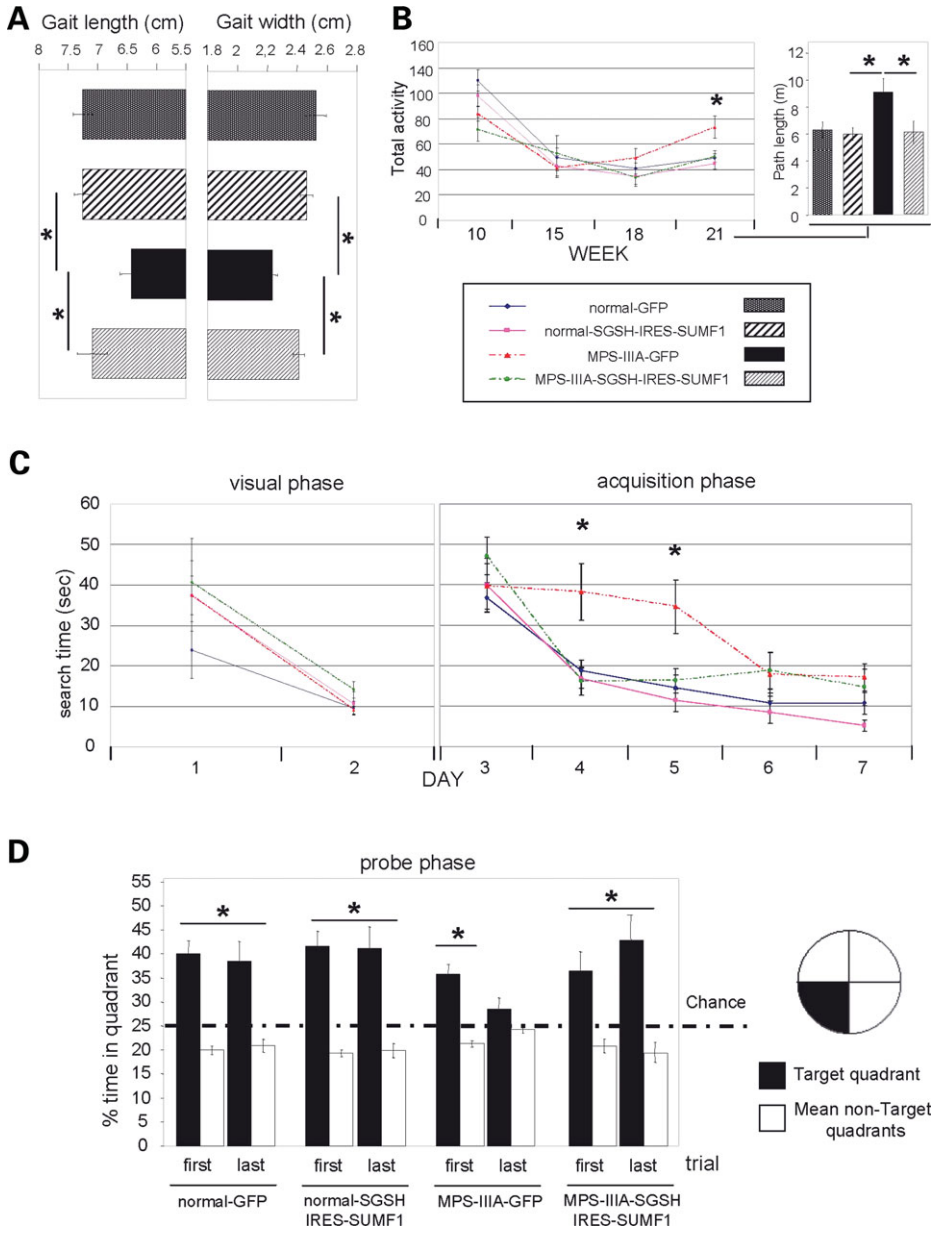

Figure 7. Testing of motor and cognitive abilities in injected mice. Male mice belonging to the four treatment groups (see legend) were subjected to different behavioral tests. (**A**) Gait length and gait width for each group were measured 18 weeks after injection and expressed as the mean over the total number of mice for that group. (**B**) The four groups of mice were tested in the open field 10, 15, 18 and 21 weeks after injection. Total activity, corresponding to the sum of the number of lines crossed and the number of rears observed during the 3 min trial, was calculated by averaging the single measurements obtained from each mouse within a group at each time point. The path length covered by each group of mice at 21 weeks of age during the 3 min trial was also measured. (**C** and **D**) MWM test at 20 weeks of age. The average time taken by each group of mice to reach the platform (search time) during the visual (days 1–2) and acquisition phases (days 3–7) is shown (C). (D) On day 8 of the MWM test, mice belonging to the four treatment groups were subjected to the probe phase. The percentage time spent by each group of mice in the target quadrant (where the platform had previously been located) and non-target quadrants during the first and last trials of the probe phase is shown. Error bars: ± 1 SEM. (* $P < 0.05$).

(GFP-treated) took a significantly longer time ($P < 0.05$) to locate the platform compared with normal (GFP- and SGSH-IRES-SUMF1-treated) mice (Fig. 7C). Conversely, the search time assessed for SGSH-IRES-SUMF1-treated MPS-IIIA mice was similar to that measured for normal mice (Fig. 7C), thus demonstrating an improvement in cognitive function in affected mice upon treatment with both SGSH and SUMF1. In the last 2 days of the acquisition phase (days 6 and 7), all mice performed similarly and no significant differences were measured in searching time (Fig. 7C). The improvement in MWM performance in MPS-IIIA mice treated with AAV expressing both SGSH and SUMF1 was confirmed in the probe (or memory) phase, performed the day after the acquisition phase ended. The analysis of each of the four trials during the probe phase showed that normal (GFP- and SGSH-IRES-SUMF1-treated)

and SGSH-IRES-SUMF1-treated MPS-IIIA mice spent a significantly ($P < 0.05$) longer time in the target quadrant compared with the other quadrants during all trials (Fig. 7D). Conversely, the GFP-treated MPS-IIIA mice that learned the position of platform during the last days of acquisition phase spent a significantly ($P < 0.05$) longer time in the target quadrant only during the first probe trial, and an equal time in each quadrant during the last trial, demonstrating a rapid loss of knowledge of the platform's location (known as extinction) (Fig. 7D).

DISCUSSION

CNS involvement in MPS-IIIA is very severe. At present, there is no therapy available for the treatment of CNS pathology in MPS-IIIA patients. Intracerebrospinal fluid enzyme delivery appears to be an effective way of delivering lysosomal enzymes to the CNS (26). However, given the invasive means by which enzyme will need to be repeatedly delivered, it is, at best, a short- to medium-term treatment option.

Gene therapy is still largely unexplored as a potential treatment for MPS-IIIA. We have utilized the MPS-IIIA mouse to demonstrate the validity of a new gene therapy approach based on the co-delivery of SGSH and SUMF1 to the lateral ventricles of neonatal mice using AAV2/5 vectors. The AAV serotype 5 has been demonstrated to be more efficient than other AAV serotypes in transducing different regions of the mammalian nervous system (27). Consistent with these studies, we found that AAV2/5-CMV-GFP targeting of the lateral ventricles in newborn mice can mediate an efficient and stable distribution of the GFP. After intraventricular microinjection, the GFP signal was not limited to areas surrounding the injection site (choroid plexus/ependyma) but extended to more distant regions, such as the cerebral cortex, hippocampus, thalamus, cerebellum and olfactory bulb. Moreover, GFP expression persisted for up to 9 months post-injection. Very high GFP expression was observed in the olfactory bulb, most likely because the subventricular zone of the lateral ventricle is the site of neural precursors that generate new olfactory bulb interneurons throughout adulthood (28).

SUMF1 was able to synergistically increase SGSH activity *in vitro* (in primary neural cells) and *in vivo* (in the brain of MPS-IIIA mice). The distribution of SGSH activity in the brain of MPS-IIIA mice injected with AAV2/5-CMV-SGSH-IRES-SUMF1 vectors was consistent with the GFP transduction pattern. The amount of enzyme detected in brain slices containing transduced areas was up to 3-fold higher than that detected in the corresponding slices of MPS-IIIA mice injected with GFP. The low enzyme activity observed in such slices can be ascribed to the presence of both transduced and untransduced areas in the brain slice. Conversely, no change in SGSH activity was observed in the brain of normal mice upon infection with AAV2/5 expressing SGSH, or both SGSH and SUMF1. We hypothesize that, in this context, the high amount of endogenous SGSH activity may have masked the contribution of the exogenously supplied enzyme. We did not undertake an ELISA to detect the presence of anti-human SGSH antibodies in samples taken from AAV-treated mice. Previous (26) and on-going studies in MPS-IIIA mice (unpublished data) suggest that the congenic strain of MPS-IIIA mice does produce anti-SGSH antibodies when treated with recombinant enzyme either intravenously from birth or when intracerebrospinal fluid delivery of enzyme begins in adulthood. The presence of the antibodies does not appear to affect the ability of the enzyme to reduce lysosomal storage and improve other pathological changes. No evidence of a cellular immune response was observed in the pathological examination of brain tissues from AAV-treated mice. Moreover, several studies have demonstrated that the use of a widely expressed promoter such as CMV or phosphoglycerate kinase in the CNS results in long-term expression of the transgene in the absence of any immune response-suppression effect (14,29,30). Our observation of long-term gene expression in AAV-treated mice is in agreement with these findings.

The amount of SGSH activity in the transduced brain areas of SGSH-IRES-SUMF1-injected MPS-IIIA mice was sufficient to obtain a stable correction of primary and secondary pathological storage over the 5-month duration of the experiments in selected brain regions. Examined histologically, the decrease in storage material appeared more evident in neurons compared with glia. This might be due to the tropism of AAV5 serotype vectors that almost exclusively transduce neurons and occasionally transduce glial cells (31). It should be highlighted that the reduction in pathological storage was only evident in the brain areas efficiently transduced by the AAV2/5 vectors (for example, striatum, cerebral cortex and olfactory bulb). In fact, when entire brain slices encompassing both AAV-containing and non-AAV-containing areas were quantitatively analyzed for pathological storage by measuring the relative amount of glucosamine-*N*-sulfate [$\alpha-1,4$]hexuronic acid (HNS-UA) in the brain extracts (9,26), no significant reduction in the level of HNS-UA was observed (Supplementary Material).

Although treatment of neural cells with AAV (encoding either SGSH or SGSH/SUMF1) resulted in a significant increase in SGSH activity in both normal and MPS-IIIA neural cells (Fig. 1A), we did not determine which type of cells were infected, or whether there were uninfected (but treated) cells in the cultures: these would presumptively have been treated via uptake of secreted enzyme. Therefore, it is not possible to definitively say that cross-correction occurred. This is consistent with the tropism of AAV5 (preferentially neuronal) and our *in vivo* observation of greater reduction in neuronal storage than glial storage following AAV treatment.

The development of inflammation in the CNS is associated with neurodegeneration in several LSDs (32–35). The underlying cause and ultimate impact of neuroinflammatory changes on disease progression in LSDs that affect the brain are not yet fully understood. Interestingly, a clinical improvement was observed in Sandhoff disease mice (36,37) when inflammatory changes within the brain were reduced in the absence of any effect on lysosomal storage. Further, synergistic effects are seen when therapies designed to reduce lysosomal storage are combined with anti-inflammatory medication (36). Our results reinforce previous observations (25), indicating that a vigorous inflammatory response also takes place throughout the brain of MPS-IIIA mice. In the present study,

we showed that the CNS of MPS-IIIA mice displayed a remarkable degree of reactive astrocytes and a large number of activated macrophages. Notably, EM analysis and MOMA-2 staining indicated that microglial cells containing storage vacuoles were often found juxtaposed to neurons from which they most likely endocytose undegraded materials. The appearance of perineuronal microglia has also been previously reported in MPS-IIIB mice (34). Treatment with AAV2/5 vectors expressing SGSH and SUMF1 significantly reduced the population of activated macrophages/microglia and astrogliosis in the CNS-transduced areas of MPS-IIIA mice.

Disease progression in MPS-IIIA mice results in severe neurodegeneration, causing both locomotor and learning dysfunction, which have been documented using a variety of behavioral tests (7,10,22). In the present study, a reduction in various aspects of neuropathology in the brain of SGSH-IRES-SUMF1-treated MPS-IIIA mice was associated with an improvement in behavioral phenotype. The injection of SGSH-IRES-SUMF1 in the brain of MPS-IIIA mice restored normal gait properties. Moreover, the increased exploratory activity displayed by GFP-treated MPS-IIIA mice following repeated open-field testing was reduced to a level similar to that observed in normal mice upon SGSH/SUMF1 treatment. Notably, the increased exploratory activity of GFP-treated MPS-IIIA mice might suggest that the affected GFP-treated mice do not remember the test arena and thus, as they age, explore the open field as if it was a new environment rather than one already explored. Finally, cognitive functions also appeared to ameliorate with SGSH/SUMF1 treatment as evidenced by the improved performance of SGSH-IRES-SUMF1-treated MPS-IIIA mice in both acquisition and probe phase of the MWM test.

In all the behavioral tests employed, the performance of normal mice treated with either AAV2/5-CMV-SGSH-IRES-SUMF1 or AAV2/5-CMV-GFP was indistinguishable, thus indicating that the change in behavior observed in MPS-IIIA mice upon treatment with AAV2/5-CMV-SGSH-IRES-SUMF1 was due to the introduction of therapeutic genes.

Although we cannot exclude the possibility that *in vivo* transduction with SGSH alone might be sufficient to provide appropriate amounts of SGSH required to improve the disease phenotype in MPS-IIIA, our results demonstrate that co-expression of SUMF1 with SGSH results in a significant enhancing effect on SGSH activity both *in vitro* and *in vivo*. Consequently, a reduction in clinical and neuropathological signs in MPS-IIIA mice can be achieved after simultaneous AAV2/5-mediated delivery of *SGSH* and *SUMF1* genes to the neonatal brain. Our findings are supported by a number of different studies that demonstrated the efficacy of AAVs in correcting the CNS pathology in MPS mouse models. For example, AAV vectors have been shown to efficiently transduce the CNS of MPS-VII mice and mediate long-term expression of transgene necessary for a therapeutic response (14,16,29). Further, CNS treatment with rAAV reversed and prevented neuropathology in MPS-I mice (15,38). Improved behavior and neuropathology were also observed in an MPS-IIIB mouse model after AAV-mediated gene transfer in the striatum (30). Interestingly, another recent study by Fu *et al*. (39) demonstrated the great potential of combining brain delivery and intravenous administration of rAAV for improving CNS pathology in MPS-IIIB mice.

In conclusion, early treatment by AAV-mediated intraventricular injection is sufficient to prevent or delay CNS pathology in MPS-IIIA mice in selected brain regions where concurrent stable expression of the transgenes was also present.

MATERIALS AND METHODS

Vector cloning and production of AAV

The pAAV-CMV-GFP and pAAV-CMV-SGSH plasmids have been described previously (21,40). To produce the pAAV-CMV-SGSH-IRES-SUMF1 vector, the GFP coding sequence in the pAAV-CMV-GFP plasmid was replaced by an IRES cassette. The SGSH and SUMF1 cDNA were then cloned, respectively, upstream and downstream of the IRES. The AAV serotype 5 (AAV2/5) vectors were produced by the AAV TIGEM Vector Core according to previously described protocols (41).

Animals

Homozygous mutant (MPS-IIIA, $-/-$) and heterozygous (phenotypically normal $+/+$ or $+/-$) congenic C57BL/6 mice were utilized (7). Consequently, the term 'normal mice' is used in this paper to refer to the mouse phenotype. Animal studies were approved by the Children, Youth and Women's Health Service Animal Ethics Committee (Adelaide, Australia) and were undertaken with respect to the guidelines of the Australian National Health and Medical Research Council for laboratory animal usage.

Primary brain cell culture and infections

Primary neural cells were obtained from newborn MPS-IIIA and normal control mice, using established protocols (Sutherland-Morizzi *et al*., submitted for publication). Cultured cells were maintained in DMEM supplemented with 5% fetal calf serum, 5% horse serum and penicillin/streptomycin. For infection, the appropriate AAV vector mix (1×10^5 viral particles/cell) was added to subconfluent cell cultures in DMEM without serum for 2 h.

Intraventricular injections and tissue collection

Newborn MPS-IIIA and normal mice at postnatal day 0 or day 1 were cryoanesthetized. The vectors (6×10^9 or 3×10^{10} particles in 1 μl) were delivered bilaterally into the lateral ventricles. Male mice were used for the behavioral tests (8–10 per group) and kept until 22 weeks of age before sacrifice. The remaining male mice, together with any female mice, were culled at 6, 12, or 22 weeks of age.

At 6 and 12 weeks of age, a total of 12 mice were sacrificed (three in each treatment group). At 22 weeks of age, a total of 24 mice were sacrificed (six in each treatment group). One mouse (at 6- and 12-week time points) or three mice (at 22-week time point) from each treatment group were perfused/fixed with 4% (w/v) paraformaldehyde in PBS. The

brain was then removed, fixed, divided into two halves along the mid-sagittal fissure and further processed for GFP analysis, immunostaining and EM analysis. The remaining mice from each treatment group were sacrificed, the brains removed and placed into a brain blocker (Braintree Scientific, Braintree, MA, USA). Each brain was then divided along the mid-line: one hemisphere was sectioned coronally into five slices ($\sim$1 mm thickness each) and samples were frozen at -70°C and processed for SGSH activity.

SGSH activity assay and mass spectrometric analysis

The cell pellets or brain slices were homogenized in 0.02 M Tris/0.5 M NaCl, pH 7.4. Samples were then subjected to six cycles of freeze/thaw and centrifuged; the supernatant was collected and processed for SGSH activity (42) or electrospray ionization tandem mass spectrometry (ESI-MS/MS), as previously described (9).

GFP analysis and immunostaining

Sagittal vibratome sections were cut at 20 μm thickness and processed for GFP analysis, immunofluorescence or immunohistochemical staining. For GM2 immunofluorescence, we adapted a protocol from McGlynn *et al*. (23). Primary antibody (polyclonal rabbit anti-GM2; Calbiochem) was diluted 1:360. For MOMA-2 immunofluorescence, we adapted a protocol from Ohmi *et al*. (34). Monoclonal rat anti-MOMA-2 (Serotech) was diluted 1:250, and polyclonal rabbit anti-GFAP was diluted 1:4000. The secondary antibodies were purchased from Molecular Probes or Jackson ImmunoResearch. Immunohistochemistry analysis was performed using Vectastain ABC kit (Vector Laboratories, Burlingame, CA, USA) according to standard protocols. Sections were mounted and coverslipped in glycerol/DAPI and viewed on an epi-fluorescent microscope or counterstained with hematoxylin and viewed on a light microscope.

Histopathological analysis of lysosomal storage

Blocks of approximately 1 mm $\times$ 2 mm $\times$ 2 mm were taken from the olfactory bulb, cerebral cortex, hippocampus and striatum of paraformaldehyde-perfused brain and subsequently processed using previously published methods (23). Ultrathin sections were visualized with a Phillips CM100 transmission electron microscope.

Behavioral procedures

All behavioral tests were performed on male mice under normal lighting conditions by the same experimenter (A.F.), using previously established protocols (7,10). All mice $\geq$15 weeks of age which underwent behavioral tests were singly caged. HVS Image software (www.hvsimage.com) was employed to quantify open-field activity and MWM performance.

Data analysis

Data are expressed as the mean $\pm$ 1 SEM. ANOVA (or RMANOVA) was used to compare different treatment groups of either mice or cells; a P-value of <0.05 was considered to be statistically significant. In the MWM test, the latency for each animal to reach the platform was considered as the dependent variable. A natural log transformation was applied to the latency data. RMANOVA was used to assess differences in latency over days, between groups and trials. Each assessment period (visual, acquisition and probe phase) was analyzed separately. The analysis was performed with SPSS v10 by Craig Hirte, Department of Public Health, University of Adelaide, and Luisa Cutillo, TIGEM.

SUPPLEMENTARY MATERIAL

Supplementary Material is available at HMG Online.

ACKNOWLEDGEMENTS

We thank Dr Aaron Robinson for assistance with injections, Dr Maria Fuller and Barbara King for ESI-MS/MS analysis, Suzie Brodie, Amanda Luck and The CYWHS Animal House staff for looking after the mice, Adelaide Microscopy for EM assistance and Dr Maria Pia Cosma for critical reading of the manuscript.

Conflict of Interest statement. An international patent is held by J.J.H. and others for mammalian sulfamidase and genetic sequences encoding it, for use in the investigation, diagnosis and treatment of subjects suspected of suffering from sulphamidase deficiency (US Patent no. 5863782). The funding sources did not have any role in study design, data collection, data analysis, interpretation of data, writing of the report or in the decision to submit the paper for publication.

FUNDING

This work was supported by the Australian NH&MRC to J.J.H., K.H., A.C. The Canadian Sanfilippo Foundation to J.J.H., the Italian Telethon Foundation to A.B. (Grant #s - not available), the Italian Ministry of Agriculture (MiPAF) and an EMBO short fellowship (ASTF 347-2005).

REFERENCES

1. Suzuki, K. (2002) Lysosomal disease. In Graham, D.I. and Lantos, P.L. (eds), *Greenfield's Neuropathology*. Arnold, London, pp. 653–735.
2. Neufeld, E.F. and Muenzer, J. (2001) The mucopolysaccharidoses. *The Metabolic and Molecular Basis of Inherited Disease*. McGraw-Hill, New York, pp. 3421–3452.
3. Meikle, P.J., Hopwood, J.J., Clague, A.E. and Carey, W.F. (1999) Prevalence of lysosomal storage disorders. *JAMA*, **281**, 249–254.
4. Fischer, A., Carmichael, K.P., Munnell, J.F., Jhabvala, P., Thompson, J.N., Matalon, R., Jezyk, P.F., Wang, P. and Giger, U. (1998) Sulfamidase deficiency in a family of Dachshunds: a canine model of mucopolysaccharidosis IIIA (Sanfilippo A). *Pediatr. Res.*, **44**, 74–82.
5. Jolly, R.D., Allan, F.J., Collett, M.G., Rozaklis, T., Muller, V.J. and Hopwood, J.J. (2000) Mucopolysaccharidosis IIIA (Sanfilippo syndrome) in a New Zealand Huntaway dog with ataxia. *N. Z. Vet. J.*, **48**, 144–148.

6. Bhaumik, M., Muller, V.J., Rozaklis, T., Johnson, L., Dobrenis, K., Bhattacharyya, R., Wurzelmann, S., Finamore, P., Hopwood, J.J., Walkley, S.U. *et al.* (1999) A mouse model for mucopolysaccharidosis type III A (Sanfilippo syndrome). *Glycobiology*, **9**, 1389–1396.
7. Crawley, A.C., Gliddon, B.L., Auclair, D., Brodie, S.L., Hirte, C., King, B.M., Fuller, M., Hemsley, K.M. and Hopwood, J.J. (2006) Characterization of a C57BL/6 congenic mouse strain of mucopolysaccharidosis type IIIA. *Brain Res.*, **1104**, 1–17.
8. Bhattacharyya, R., Gliddon, B., Beccari, T., Hopwood, J.J. and Stanley, P. (2001) A novel missense mutation in lysosomal sulfamidase is the basis of MPS III A in a spontaneous mouse mutant. *Glycobiology*, **11**, 99–103.
9. King, B., Savas, P., Fuller, M., Hopwood, J. and Hemsley, K. (2006) Validation of a heparan sulfate-derived disaccharide as a marker of accumulation in murine mucopolysaccharidosis type IIIA. *Mol. Genet. Metab.*, **87**, 107–112.
10. Hemsley, K.M. and Hopwood, J.J. (2005) Development of motor deficits in a murine model of mucopolysaccharidosis type IIIA (MPS-IIIA). *Behav. Brain. Res.*, **158**, 191–199.
11. Vogler, C., Levy, B., Grubb, J.H., Galvin, N., Tan, Y., Kakkis, E., Pavloff, N. and Sly, W.S. (2005) Overcoming the blood-brain barrier with high-dose enzyme replacement therapy in murine mucopolysaccharidosis VII. *Proc. Natl Acad. Sci. USA*, **102**, 14777–14782.
12. Hildinger, M. and Auricchio, A. (2004) Advances in AAV-mediated gene transfer for the treatment of inherited disorders. *Eur. J. Hum. Genet.*, **12**, 263–271.
13. Xiao, X., Li, J., McCown, T.J. and Samulski, R.J. (1997) Gene transfer by adeno-associated virus vectors into the central nervous system. *Exp. Neurol.*, **144**, 113–124.
14. Sferra, T.J., Qu, G., McNeely, D., Rennard, R., Clark, K.R., Lo, W.D. and Johnson, P.R. (2000) Recombinant adeno-associated virus-mediated correction of lysosomal storage within the central nervous system of the adult mucopolysaccharidosis type VII mouse. *Hum. Gene Ther.*, **11**, 507–519.
15. Desmaris, N., Verot, L., Puech, J.P., Caillaud, C., Vanier, M.T. and Heard, J.M. (2004) Prevention of neuropathology in the mouse model of Hurler syndrome. *Ann. Neurol.*, **56**, 68–76.
16. Liu, G., Martins, I., Wemmie, J.A., Chiorini, J.A. and Davidson, B.L. (2005) Functional correction of CNS phenotypes in a lysosomal storage disease model using adeno-associated virus type 4 vectors. *J. Neurosci.*, **25**, 9321–9327.
17. Cosma, M.P., Pepe, S., Annunziata, I., Newbold, R.F., Grompe, M., Parenti, G. and Ballabio, A. (2003) The multiple sulfatase deficiency gene encodes an essential and limiting factor for the activity of sulfatases. *Cell*, **113**, 445–456.
18. Dierks, T., Schmidt, B., Borissenko, L.V., Peng, J., Preusser, A., Mariappan, M. and von Figura, K. (2003) Multiple sulfatase deficiency is caused by mutations in the gene encoding the human C(alpha)-formylglycine generating enzyme. *Cell*, **113**, 435–444.
19. Settembre, C., Annunziata, I., Spampanato, C., Zarcone, D., Cobellis, G., Nusco, E., Zito, E., Tacchetti, C., Cosma, M.P. and Ballabio, A. (2007) Systemic inflammation and neurodegeneration in a mouse model of multiple sulfatase deficiency. *Proc. Natl Acad. Sci. USA*, **104**, 4506–4511.
20. Kurai, T., Hisayasu, S., Kitagawa, R., Migita, M., Suzuki, H., Hirai, Y. and Shimada, T. (2007) AAV1 mediated co-expression of formylglycine-generating enzyme and arylsulfatase A efficiently corrects sulfatide storage in a mouse model of metachromatic leukodystrophy. *Mol. Ther.*, **15**, 38–43.
21. Fraldi, A., Biffi, A., Lombardi, A., Visigalli, I., Pepe, S., Settembre, C., Nusco, E., Auricchio, A., Naldini, L., Ballabio, A. *et al.* (2007) SUMF1 enhances sulfatase activities *in vivo* in five sulfatase deficiencies. *Biochem. J.*, **403**, 305–312.
22. Gliddon, B.L. and Hopwood, J.J. (2004) Enzyme-replacement therapy from birth delays the development of behavior and learning problems in mucopolysaccharidosis type IIIA mice. *Pediatr. Res.*, **56**, 65–72.
23. McGlynn, R., Dobrenis, K. and Walkley, S.U. (2004) Differential subcellular localization of cholesterol, gangliosides, and glycosaminoglycans in murine models of mucopolysaccharide storage disorders. *J. Comp. Neurol.*, **480**, 415–426.
24. Leenen, P.J., de Bruijn, M.F., Voerman, J.S., Campbell, P.A. and van Ewijk, W. (1994) Markers of mouse macrophage development detected by monoclonal antibodies. *J. Immunol. Methods*, **174**, 5–19.
25. Savas, P.S., Hemsley, K.M. and Hopwood, J.J. (2004) Intracerebral injection of sulfamidase delays neuropathology in murine MPS-IIIA. *Mol. Genet. Metab.*, **82**, 273–285.
26. Hemsley, K.M., King, B. and Hopwood, J.J. (2007) Injection of recombinant human sulfamidase into the CSF via the cerebellomedullary cistern in MPS IIIA mice. *Mol. Genet. Metab.*, **90**, 313–328.
27. Burger, C., Nash, K. and Mandel, R.J. (2005) Recombinant adeno-associated viral vectors in the nervous system. *Hum. Gene Ther.*, **16**, 781–791.
28. Luskin, M.B. (1993) Restricted proliferation and migration of postnatally generated neurons derived from the forebrain subventricular zone. *Neuron*, **11**, 173–189.
29. Bosch, A., Perret, E., Desmaris, N. and Heard, J.M. (2000) Long-term and significant correction of brain lesions in adult mucopolysaccharidosis type VII mice using recombinant AAV vectors. *Mol. Ther.*, **1**, 63–70.
30. Cressant, A., Desmaris, N., Verot, L., Brejot, T., Froissart, R., Vanier, M.T., Maire, I. and Heard, J.M. (2004) Improved behavior and neuropathology in the mouse model of Sanfilippo type IIIB disease after adeno-associated virus-mediated gene transfer in the striatum. *J. Neurosci.*, **24**, 10229–10239.
31. Burger, C., Gorbatyuk, O.S., Velardo, M.J., Peden, C.S., Williams, P., Zolotukhin, S., Reier, P.J., Mandel, R.J. and Muzyczka, N. (2004) Recombinant AAV viral vectors pseudotyped with viral capsids from serotypes 1, 2 and 5 display differential efficiency and cell tropism after delivery to different regions of the central nervous system. *Mol. Ther.*, **10**, 302–317.
32. Wada, R., Tifft, C.J. and Proia, R.L. (2000) Microglial activation precedes acute neurodegeneration in Sandhoff disease and is suppressed by bone marrow transplantation. *Proc. Natl Acad. Sci. USA*, **97**, 10954–10959.
33. Jeyakumar, M., Thomas, R., Elliot-Smith, E., Smith, D.A., van der Spoel, A.C., d'Azzo, A., Perry, V.H., Butters, T.D., Dwek, R.A. and Platt, F.M. (2003) Central nervous system inflammation is a hallmark of pathogenesis in mouse models of GM1 and GM2 gangliosidosis. *Brain*, **126**, 974–987.
34. Ohmi, K., Greenberg, D.S., Rajavel, K.S., Ryazantsev, S., Li, H.H. and Neufeld, E.F. (2003) Activated microglia in cortex of mouse models of mucopolysaccharidoses I and IIIB. *Proc. Natl Acad. Sci. USA*, **100**, 1902–1907.
35. Baudry, M., Yao, Y., Simmons, D., Liu, J. and Bi, X. (2003) Postnatal development of inflammation in a murine model of Niemann–Pick type C disease: immunohistochemical observations of microglia and astroglia. *Exp. Neurol.*, **184**, 887–903.
36. Jeyakumar, M., Smith, D.A., Williams, I.M., Borja, M.C., Neville, D.C., Butters, T.D., Dwek, R.A. and Platt, F.M. (2004) NSAIDs increase survival in the Sandhoff disease mouse: synergy with *N*-butyldeoxynojirimycin. *Ann. Neurol.*, **56**, 642–649.
37. Denny, C.A., Kasperzyk, J.L., Gorham, K.N., Bronson, R.T. and Seyfried, T.N. (2006) Influence of caloric restriction on motor behavior, longevity, and brain lipid composition in Sandhoff disease mice. *J. Neurosci. Res.*, **83**, 1028–1038.
38. Watson, G., Bastacky, J., Belichenko, P., Buddhikot, M., Jungles, S., Vellard, M., Mobley, W.C. and Kakkis, E. (2006) Intrathecal administration of AAV vectors for the treatment of lysosomal storage in the brains of MPS I mice. *Gene Ther.*, **13**, 917–925.
39. Fu, H., Kang, L., Jennings, J.S., Moy, S.S., Perez, A., Dirosario, J., McCarty, D.M. and Muenzer, J. (2007) Significantly increased lifespan and improved behavioral performances by rAAV gene delivery in adult mucopolysaccharidosis IIIB mice. *Gene Ther.*, **14**, 1065–1077.
40. Auricchio, A., Kobinger, G., Anand, V., Hildinger, M., O'Connor, E., Maguire, A.M., Wilson, J.M. and Bennett, J. (2001) Exchange of surface proteins impacts on viral vector cellular specificity and transduction characteristics: the retina as a model. *Hum. Mol. Genet.*, **10**, 3075–3081.
41. Auricchio, A., Hildinger, M., O'Connor, E., Gao, G.P. and Wilson, J.M. (2001) Isolation of highly infectious and pure adeno-associated virus type 2 vectors with a single-step gravity-flow column. *Hum. Gene Ther.*, **12**, 71–76.
42. Karpova, E.A., Voznyi Ya, V., Keulemans, J.L., Hoogeveen, A.T., Winchester, B., Tsvetkova, I.V. and van Diggelen, O.P. (1996) A fluorimetric enzyme assay for the diagnosis of Sanfilippo disease type A (MPS IIIA). *J. Inherit. Metab. Dis.*, **19**, 278–285.